Proton Emission from Cone-in-Shell Fast-Ignition Experiments at the Omega Laser Facility

Introduction

The fast-ignition concept[1,2] has been described thoroughly in literature as one alternative to direct-drive hot-spot ignition. In this scheme a high-energy, high-intensity (10^{15} W/cm^2) laser is used to compress a cold shell containing fusion fuel to high areal densities ($\rho R \sim 1$ g/cm^2). A short-pulse, ultrahigh-intensity laser (10^{19} W/cm^2) is then used to generate megavolt electrons to heat the core of the dense fuel assembly in a time that is short compared to hydrodynamic time scales. The use of two independent laser drivers to compress the fuel assembly and subsequently heat the core allows for higher target gains, in principle, for the same amount of driver energy. This is because high fuel-areal-density cores can be assembled with slow implosion velocities and ignition is achieved by efficiently coupling the short-pulse beam energy to the dense core.[1] In comparison to conventional hot-spot ignition, the symmetry requirement of the fuel assembly in fast ignition is not as stringent; this relaxes the illumination uniformity and power-balance constraints of the driver.

The success of this approach relies on the effective energy coupling between the short-pulse laser and the pre-assembled dense fuel. A high coupling efficiency (CE) depends on the generation of hot electrons and their transport and energy deposition to the dense fuel core. A potential problem is that the generation of energetic electrons will also inevitably accelerate ions. Any energy coupling to ions is a direct-loss channel that must be examined.

The acceleration of ions, and in particular protons, by electrostatic sheath fields set up by hot electrons generated by laser–plasma interaction (LPI) has been observed in both direct-drive[3] and indirect-drive[4] configurations with high-intensity (~10^{14}-W/cm^2) long-pulse beams. Protons and heavier ions produced by ultra-intense (~10^{18} to 10^{19} W/cm^2) short-pulse laser–plasma interactions have also been studied extensively using flat-foil and cone targets. In short-pulse scenarios, laser-to-proton energy conversion efficiency, angular emission of protons from flat-foil targets, focused emission of proton beams, and effects of plasma scale length on proton acceleration have been studied.[5–7] Proton measurements have also been used, in conjunction with ion expansion models,[8–10] to infer the temperature of the LPI-generated hot-electron distribution that accelerates these protons.[11,12]

This article presents the first measurements of fast protons in surrogate cone-in-shell fast-ignitor experiments conducted at the Omega Laser Facility.[13,14] In these experiments, a short-pulse laser was focused into gold cones to generate hot electrons and subsequently heat a pre-assembled dense D_2 core, with the aim to increase the DD-neutron yield by raising the ion temperature.[15] For these experiments, the neutron-yield enhancement caused by core heating has been measured to be a factor of ~4, corresponding to a CE of 3.5% (Ref. 15).

In the context of proton acceleration, these experiments differ from previous work with cone targets and short-pulse lasers in that protons have been used here as a diagnostic tool to (1) assess effectiveness of fast-ignitor coupling to the dense core and (2) determine the energy coupling to protons, a loss mechanism in fast-ignition experiments.

The following sections provide an overview of the experimental setup and charged-particle diagnostics used to measure proton spectra; present proton spectra and maximum energies; discuss where and how the protons are generated; and relate how protons are used to infer the hot-electron temperature for these experiments. The article concludes with a summary of results.

Experiments

The experiments were performed at LLE using both the OMEGA (long-pulse) and OMEGA EP (short-pulse) lasers. OMEGA is a 60-beam neodymium-glass laser capable of focusing 30 kJ of frequency-tripled light at a wavelength of 351 nm to on-target intensities greater than 10^{15} W/cm^2. OMEGA EP consists of four beams, two of which are short pulse, each capable of delivering 1 kJ of 1053-nm light in 10 ps, while the other two are long pulse. In these experiments,[15] 54 OMEGA beams delivering 18 kJ of UV light to the capsule were used to compress the target along a low adiabat ($\alpha \approx 1.5$), which

was achieved using a short single picket, followed by a main drive pulse with a duration of approximately 2.7 ns. A single short-pulse (~10-ps), Gaussian-shaped OMEGA EP beam was then brought to focus inside the OMEGA target chamber. At best focus, 80% of the beam energy was contained within a diameter of approximately 50 μm, resulting in a maximum, beam-averaged on-target intensity of $\approx 6 \times 10^{18}$ W/cm^2. For these experiments, the OMEGA EP power and energy contrast were of the order of 10^6 and 10^4, respectively.[15] Details on the targets can also be found in Ref. 15. In summary, the targets for these experiments were re-entrant gold cones inside 40-μm-thick, deuterated-plastic (CD) shells with a nominal diameter of 870 μm. The cones were either 1.2 or 1.8 mm in length and had an opening half-angle of 17°. The cone tips were flat with a variable tip thickness (5 to 15 μm) and a tip diameter of 10 μm. The cone walls were 10 μm thick inside the shell and 50 μm thick outside. The shells were not gas filled, leaving only the CD shell and the ablated material from it to undergo fusion.

Proton energy spectra were measured using both magnet-based charged-particle spectrometers (CPS1 and CPS2) and wedged-range-filter (WRF) spectrometers.[16] These instruments utilize CR-39 solid-state nuclear track detectors (SSNTD's), which are known to provide information about the energy and species of the detected charged particles.[16] It has been shown recently, however, that there exists CR-39 piece-to-piece variability in its response to charged particles.[17] Therefore, CR-39 alone cannot be used to accurately measure charged-particle spectra and must be paired with an additional particle dispersion mechanism. In addition, CR-39 is immune to electromagnetic pulse and, to some extent, to x rays, making it ideal for short-pulse experiments such as those presented here.

The CPS's feature a 0.1-mm slit and a 7.6-kG magnet to disperse charged particles onto CR-39 detectors. These spectrometers are capable of measuring proton energy spectra in the range of 200 keV to 30 MeV. The low-energy limit is set by filtering (directly in front of the CR-39), which is required to mitigate a very large flux of low-energy charged particles that would otherwise scatter within the diagnostic and saturate the detector. The high-energy limit is set by the magnet dispersion and detector arrangement. The CPS systems are fixed to the OMEGA target chamber at two different polar angles, as shown in Fig. 132.21. In practice, the exponential energy spectra of short-pulse accelerated protons result in a large on-detector proton fluence at lower energies. This may cause saturation of the CR-39 detector at these energies, effectively raising the low-energy limit of this diagnostic. It is worth noting that the CPS cannot resolve heavy ions because of the degeneracy between charge state, mass, and energy that exists for magnetic spectrometers.[16] Filters constructed of mylar and aluminum are overlaid on the CR-39 to filter out these ions. Furthermore, any energetic heavy ions that penetrate the filters are separated from protons on the basis of the contrast and diameter of the tracks they leave on the CR-39.

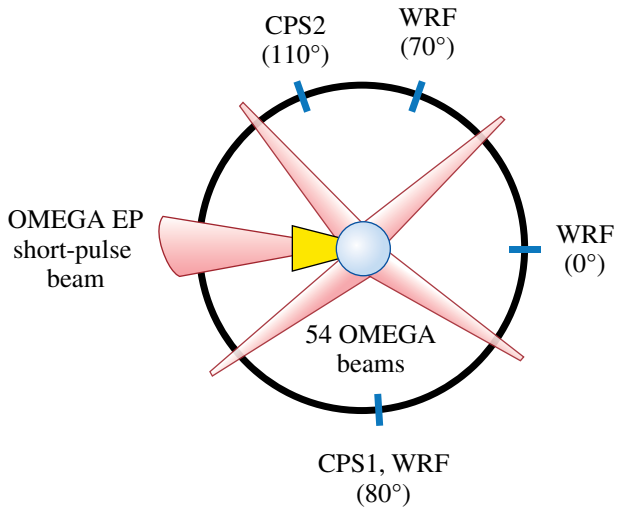

Figure 132.21
Schematic of the experimental setup. The charged-particle spectrometers (CPS1 and CPS2) and wedged-range-filter (WRF) spectrometers positioned at different azimuthal angle were used in these experiments. The coordinate system is defined such that the pole (0°) corresponds to the direction of the short-pulse laser. The OMEGA beams were used to first compress the CD shell, after which the short-pulse OMEGA EP beam was used to produce energetic electrons to heat the deuterium fuel.

The WRF spectrometers use CR-39 overlaid with a piece of wedge-shaped zirconia ceramic (ZrO_2), in which the minimum particle energy required to penetrate the wedge varies along the thickness (dispersion) direction. Since the zirconia wedge cannot be made thinner than 40 μm, the low-energy instrument cutoff for measurement of protons is approximately 3 to 4 MeV. The WRF's are compact (5 cm across) spectrometers that are ideal in probing the implosion at several locations. Several (either three or five) WRF modules, each consisting of two WRF's, were used at a single measurement location to obtain good statistics. Figure 132.21 shows the azimuthal projection of these spectrometers in the OMEGA target chamber relative to the short-pulse beam and target. The coordinate system is defined such that the pole (0°) corresponds to the direction of the short-pulse laser.

The WRF spectrometers were the primary proton diagnostic. They were fielded on nearly every shot, while the CPS was fielded on a handful of shots to corroborate the WRF measurements and provide additional details of the spectrum at energies below the WRF low-energy cutoff. The spectrometers were pointed to the target chamber center, which coincides with the center of the spherical shell. The spectrometers also subtend small solid angles (1 μsr for the CPS and 100 μsr for the WRF). As a result, they measured protons accelerated normal to the CD shell surface for each of the locations shown in Fig. 132.21. In addition, when fielded at 70° and 80°, the spectrometers measured protons accelerated nearly normal to the cone surface since that surface is nearly parallel to the spectrometer aperture because of the 17° cone opening half-angle.

Proton Spectra and Maximum Energies

A typical proton energy spectrum from integrated experiments, acquired using CPS1 (OMEGA shot 56971), is shown in Fig. 132.22. Alongside this spectrum is the proton spectrum for a neutron reference implosion (OMEGA shot 56976), where a similar target was imploded using the same long-pulse configuration (~20 kJ, 54 OMEGA beams) without any short-pulse core heating. It has been well established that long-pulse LPI generates protons up to ~1 MeV (Refs. 3 and 18), consistent with the data shown from the reference implosion. Nearly all of the observed energetic protons, however, arise from short-pulse LPI. These spectra exhibit a high-energy cutoff corresponding to the maximum path-integrated electric fields seen by the ions.

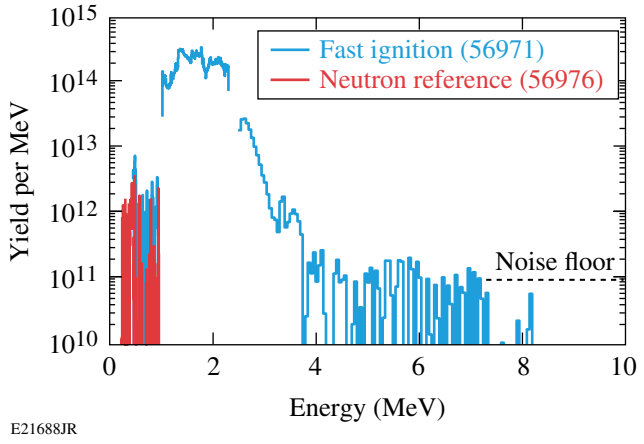

Figure 132.22
Proton spectra measured with CPS1 (80°) on fast-ignition experiments and neutron reference experiments. In both cases, a gold cone-in-shell target was compressed using 54 OMEGA beams (~20 kJ) and a low-adiabat laser drive. For the fast-ignition case, the OMEGA EP short-pulse laser was fired, at peak compression of the target, to generate hot electrons and heat the dense core. These energy spectra were background subtracted, although some residual background is observed in the 4- to 7-MeV range. The gaps in the spectrum at ~1 MeV and ~2.3 MeV are due to the instrument.

Proton energy spectra were measured down to approximately 200 keV using the CPS. As proton emission was anisotropic, it was difficult to precisely measure the total energy lost to protons. On the basis of measurements such as the one shown in Fig. 132.22, we estimate that the total energy carried by these protons is typically of the order of 10 J, or just about 1% of the incident short-pulse laser energy. This number can be compared to the previously inferred 20% coupling efficiency of short-pulse laser energy to hot electrons.[19] Therefore, approximately 5% of the short-pulse laser energy coupled to hot electrons is lost to the acceleration of ions.

The fact that the observed ions were protons (and not deuterons or heavier ions) was confirmed by simultaneous charged-particle measurements using CPS and WRF spectrometers. Since the CPS's use magnetic fields for ion dispersion, it can be shown that the inferred energy of an ion depends inversely on the assumed ion mass.[16] Therefore, the CPS-inferred energy of a deuteron mistakenly identified as a proton will be twice as large as the actual particle's energy. The WRF's have an opposite energy-mass dependence, whereby the inferred energy of a deuteron mistakenly identified as a proton will be lower than the actual particle's energy. It is therefore possible to constrain the particle species using these measurement techniques on the same shot and same polar angle. In particular, CPS1 and the WRF's measure particles at the same polar angle (80°) but different azimuthal angles.

Since the target is composed of a CD shell and Au cone, these protons originate predominantly from hydrocarbon contaminants on the surface of the target. The implications are that the protons do not significantly interact or scatter with the compressed shell. The cone-in-shell target conditions at the time when the short-pulse laser interacts with the cone are schematically illustrated in Fig. 132.23, which shows the cone, the compressed D_2 core (~50-μm diameter), the blowoff plasma surrounding the core, the generated hot electrons, and the accelerated surface protons. The relative timing between the short-pulse laser and the start of the long-pulse compression lasers was varied from shot to shot, but it is typically 3 ns. At this point in time, the blowoff plasma from the ablated shell has expanded for this same amount of time at the ion sound speed $\left(c_s \equiv \sqrt{T/m_i}\right)$, resulting in a characteristic scale length of about 400 μm to 1 mm for typical coronal temperatures of ~2 keV. The blowoff plasma scale length is therefore comparable to the length of the cone, and it is expected that the

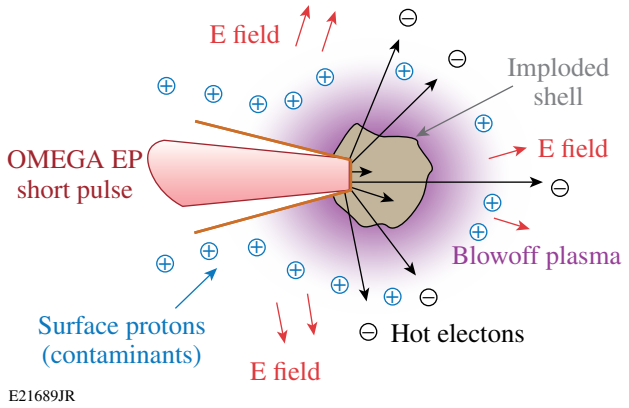

Figure 132.23
Schematic of the target conditions when the short-pulse OMEGA EP laser interacts with the cone tip. The CD shell has been compressed to a diameter of ~50 μm and is surrounded by blowoff plasma from the ablated shell (~1-mm scale length). Interaction of the short-pulse laser with the cone generates hot electrons that accelerate surface-contaminant protons from the ablated plasma.

protons from the target are accelerated in the presence of this long-scale-length plasma.

The maximum proton energy for each shot is of interest since it scales directly with the temperature of short-pulse–generated hot electrons.[20,21] Direct measurements of the maximum energy can therefore be used to qualitatively infer how the hot-electron temperature varies with experimental parameters. The maximum proton energy was measured at various locations around the implosion using the compact WRF spectrometers on several shots (Fig. 132.24). These data incorporate measurements from gold cones with 5-μm-, 10-μm-, and 15-μm-thick tips and 10-μm tip diameters. The data obtained in the direction transverse to the short-pulse beam (80° and 70°) scale with intensity. A χ^2 analysis of the data indicates that these data fit a normalized ponderomotive scaling ($\propto I^{1/2}$) at both 80° (reduced $\chi^2 = 0.96$) and 70° (reduced $\chi^2 = 0.71$). This is further confirmation that these protons are accelerated by short-pulse–generated hot electrons. In addition, since the maximum energies scale with intensity as expected from theory, these protons can be used to estimate a hot-electron temperature, albeit with some caveats (see **Inferred Hot-Electron Temperature**, p. 209).

In contrast to the transverse direction, the maximum energies of forward-going protons (0°) show neither such scaling nor a dependence on cone-tip thickness. In addition, the maximum energies of forward-going protons are lower compared to the transverse-going protons. This is consistent with simulations, which indicate that for these experiments, the hot electrons are emitted in two lobes with half-angles of 57° (with a minimum

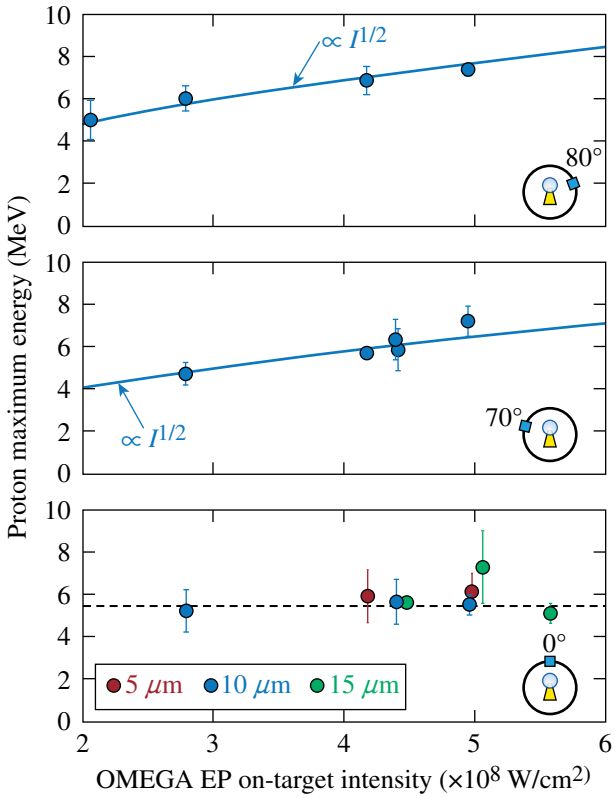

Figure 132.24
Maximum proton energies measured by WRF spectrometers at 80°, 70°, and 0° with respect to the forward short-pulse beam direction. The data points shown are averages over many WRF measurements at one location. The error bars (within 95% confidence limits) were computed from the standard deviation of these multiple measurements. At both 80° and 70°, the data show reasonable agreement with the known ponderomotive hot-electron scaling. The maximum proton energies for the forward beam direction (0°) show neither scaling with intensity nor dependence on cone-tip thickness.

in the forward direction).[22] In this case, it is expected that fewer and less-energetic protons would be observed in the forward direction even when the cone tip is intact, which is consistent with these observations.

In addition, forward-going protons are accelerated by hot electrons that have interacted with the compressed core and lost a significant amount of energy (Fig. 132.23). Some of the slower electrons are even ranged out in the core. The inferred electron temperatures and ρR of the compressed shell (~150 mg/cm^2) are consistent with this notion, as discussed further in **Inferred Hot-Electron Temperature**, p. 209. As a result, the distribution of forward-going electrons has a lower maximum energy and empty regions in velocity space, thereby reducing the energies of forward-going protons relative to transverse protons.

Several WRF's were used to obtain the average maximum proton energies at each location. The standard deviations of these measurements were used to compute the error bars (within 95% confidence limits) shown in Fig. 132.24. Since the spatial separation between adjacent WRF's is of the order of several centimeters, the observed uncertainties in the data arise from both the absolute measurement uncertainty of each WRF (~200 to 300 keV) and possible spatial variations in the maximum energy. For the case of forward-going protons, the uncertainties are as large as ±2 MeV, which is larger than the absolute measurement uncertainty of the WRF spectrometers. Therefore, we conclude that there are real spatial modulations of the maximum proton energy for forward-going protons. These observed larger spatial variations could be the reason why the scaling with intensity is not readily apparent. Furthermore, these variations are consistent with the presence of a stochastic process, such as hot electrons scattering in the compressed shell. For these reasons, it is difficult to infer a hot-electron temperature from forward-going protons, as additional physics must be unfolded from the proton measurement, and we defer to only transverse-going protons when inferring hot-electron temperatures in **Inferred Hot-Electron Temperature**, p. 209.

Source of the Protons

There is evidence that the observed protons are accelerated from the cone walls rather than from the cone tip, where the laser interacts with the cone. The data presented throughout this article consist primarily of cones 1.2 mm in length, with 10-μm or 40-μm tip diameters and variable tip thicknesses. On a few shots, cones with a length of 1.8 mm (but otherwise identical) were also shot. A comparison of 1.2-mm and 1.8-mm cones showed that the proton yields scale with the square of cone length (and therefore the surface area of the cone, for a fixed cone-opening angle). This suggests that the protons are accelerated from the entire surface of the cone rather than from the tip alone. Since charged-particle spectra were not available for these shots, proton yields could not be directly measured. Instead, relative proton yields were inferred from the neutron time-of-flight (nTOF) data in Fig. 132.25, which shows the raw signals from the nTOF liquid scintillator.[23] For these two shots, the nTOF settings, laser drive, and target parameters were identical with the exception of the cone length. The x-ray flash, which occurs when the short-pulse beam hits the cone, and the 2.45-MeV DD-neutron signals are characteristic of these implosions, as shown in Fig. 132.25. In between these signals are a number of smaller peaks associated with neutrons from (p,n) reactions in the surrounding material. Their arrival time is generally consistent with the maximum energies of the protons

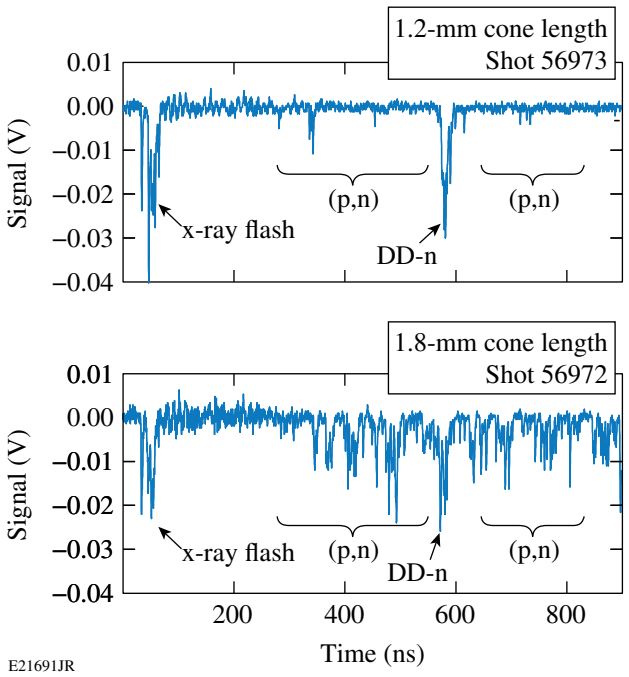

Figure 132.25
Neutron time-of-flight signal (Channel 2), showing the x-ray flash, 2.45-MeV DD-n signal, and neutrons from (p,n). For these two shots, all laser and target parameters were identical with the exception of the cone length, which was 50% greater, corresponding to 2.25× more surface area. The ratio of the total (p,n) signal of these two cone lengths is ~2 to 3, roughly proportional to the ratio of the cone surface areas. This suggests that the protons are emitted over the entire cone surface as opposed to just the tip alone.

shown in **Proton Spectra and Maximum Energies** (p. 206). The integral of these signals from the proton-arrival time (e.g., ~300 ns for 7.5-MeV protons) through 900 ns (excluding the DD-n peak) was computed for three shots: two with 1.2-mm cones and one with a 1.8-mm cone. The ratio of the integrals between the 1.2- and 1.8-mm cones' data were found to be 2.0±0.5 and 3.0±0.3, respectively. These ratios are comparable to the increase in surface area of the two cones (an increase of 2.25×). Since the number of (p,n) neutrons and, therefore, fast protons scale with the area of the cone, it is likely that they are accelerated over the entire surface of the cone.

Throughout the course of these experiments, the timing between the long-pulse OMEGA and short-pulse OMEGA EP beams was varied to find the optimal timing of the OMEGA EP beam for maximum core heating and yield. Optimal timing corresponds to core heating at peak compression of the cold, dense core.[15] For effective coupling of the short-pulse laser energy to the dense core, the cone tip must be intact when the

short-pulse laser is fired. Shock waves launched into the fuel during compression by the long-pulse OMEGA lasers will eventually reach the cone tip, break through, and leave the tip physically destroyed.[15] In this scenario, we expect poor hot-electron production, and, therefore, less-energetic protons. The cone tip was intact for the data shown in Fig. 132.24. For two shots, the timing between OMEGA and OMEGA EP was such that the tip was broken when the short pulse arrived at the tip. Figure 132.26 shows data taken at 80° using CPS1, alongside data from WRF's (80°) and CPS2 (110°). The CPS1 data are generally in excellent agreement with the WRF data. This is expected since these instruments are at the same polar angle. The two shots where the tip was broken are indicated by the open circles; WRF's were not fielded at 80° for these shots. The maximum proton energies were significantly lower (~40%) at 80° and 70° (not shown) when the tip was not intact.

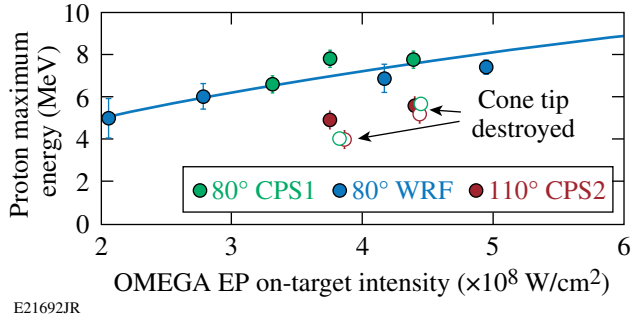

Figure 132.26
Maximum proton energies measured by CPS1, CPS2, and WRF's. The different CPS1 and WRF measurements (at 80°) show good agreement with one another, despite the fact that they sample different azimuthal angles. The solid line is a fit to the data ($\propto I^{1/2}$, with reduced $\chi^2 = 0.72$). The maximum energies of the transverse protons depend on whether the cone tip is intact when the OMEGA EP short-pulse laser arrives at the tip. When not intact (open circles), the maximum energy of the transverse protons (and therefore the fields that accelerate them) are smaller and similar to measurements and large angles (110°), as shown by the CPS2 measurement.

Since the acceleration of transverse-going protons upstream of the cone tip is affected by the presence of the tip, these data suggest that return currents associated with the initial hot-electron production could be responsible for the acceleration of these protons. We speculate that destruction of the tip affects the formation of return currents and could mitigate proton acceleration.

The drastic effect of the cone tip's destruction on electron production and subsequent proton acceleration was not observed in the forward direction, as shown in Fig. 132.27. For two shots, the 10-μm-thick cone tip was shocked before the

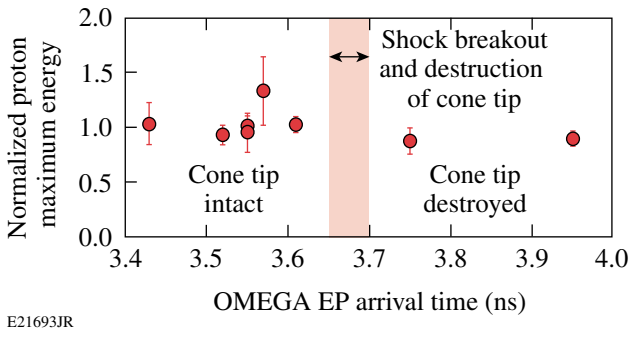

Figure 132.27
Maximum energies of forward-going protons as a function of the OMEGA EP arrival time at the cone tip relative to the start of the long-pulse drive. For comparison, the maximum energies were normalized to the mean of the data shown. Forward-going protons show no significant dependence on whether the cone tip is intact when the OMEGA EP short-pulse laser arrives at the cone tip. The shock-breakout time at the cone tip, which depends on cone-tip thickness, occurs between 3.65 ns and 3.7 ns, as shown schematically.

short pulse arrived at the cone tip. The previously measured shock-breakout time,[15] which varies with tip thickness, is indicated in Fig. 132.27. Therefore, neither the presence of the cone tip nor the thickness of the tip (per Fig. 132.24) affects the acceleration in the forward direction.

Inferred Hot-Electron Temperature

It has been suggested that the presence of a significant preformed plasma inside the cone can lead to filamentation and self-focusing of the short-pulse laser, leading to higher hot-electron temperatures.[15,24] In particular, simulations suggest that for these experiments, a preformed plasma with a scale length of 100 μm is present within the cone at the arrival time of the short-pulse OMEGA EP laser. The large preformed plasma, if present, is due to the laser prepulse that arises from amplified spontaneous emission (ASE). The prepulse is characterized by the laser contrast, defined as the amplitude ratio of the main drive to the prepulse.

Hotter electron temperatures, due to either self-focusing or another physical mechanism, result in more-energetic electrons that would not stop in the core as intended, thereby lowering the overall CE. The average ρR for spherical implosions with comparable laser and target parameters has been previously measured to be approximately 150 mg/cm^2 (Ref. 25). Given this dense core, electrons generated on one side near the cone tip would need energies of 500 keV to penetrate and escape the core, thereby accelerating surface ions in the forward direction. Therefore, we require temperatures of a few hundred kilo-electron volts, which are the expected temperatures in these experiments given the on-target intensities and the ponderomo-

tive scaling.[24] Using the proton data presented in this work, we can place a lower bound on the initial hot-electron temperature to see whether the electrons are hotter than expected from the ponderomotive scaling. The hot-electron temperature is inferred using a plasma expansion model, which links the temperature of an initial hot-electron distribution to the proton maximum energies measured here (80°). In particular, $E_M = \alpha T_H$ (Ref. 21), where α depends on the expansion model.[8–10,26] In general, α has a logarithmic dependence on the hot-electron density (n_0) and the laser pulse duration. The expansion process can be described as isothermal, adiabatic, or two phase, as described shortly. The choice of an appropriate model depends only on the relative time scales of the laser-pulse duration (τ_L) and the transit time of electrons through the target (τ_e) (Ref. 9). For these experiments, $\tau_L \sim 20\ \tau_e$. Therefore, during the first part of the laser pulse, the cone tip is completely populated with hot electrons generated from the preformed plasma on the inside of the cone. For the remainder of the pulse duration, the laser maintains the temperature of these electrons. After the pulse turns off, the electrons expand adiabatically, giving their energy to the ions. A one-dimensional (1-D) fluid model has been previously used to describe this process. This so-called two-phase fluid model[9,26] treats the laser as a source term that acts to maintain a steady temperature during the pulse (isothermal expansion) and then conserves energy between electrons, ions, and the accelerating field thereafter (adiabatic expansion).

The two-phase model relates the hot-electron temperature to the maximum proton energy by the relation

$$T_H = E_M \times \left[2.5 + 0.92 \ln\left(\omega_{pi}\tau_L\right)\right]^{-1}, \qquad (1)$$

where T_H, E_M, ω_{pi}, and τ_L are the hot-electron temperature, maximum proton energy, ion plasma frequency [$\omega_{pi} \equiv (n_{e0}e^2/m_p\varepsilon_0)^{1/2}$], and the laser-pulse duration, respectively. This formula was interpolated from numerical simulations[26] and applies for $\omega_{pi}\tau_L$ in the range of 5 to 100. The maximum energies and laser-pulse duration were measured for each shot, while the plasma frequency was estimated. To estimate n_{e0} and therefore ω_{pi}, we used a variation of a known method.[11] First, we determined the number of hot electrons generated by the short-pulse laser. Recent experiments on OMEGA EP showed that the laser-energy conversion efficiency to hot electrons is 20% for such kilojoule-class short-pulse lasers,[19] and is independent of the laser intensity. The number of hot electrons is then found by dividing the energy converted to hot electrons by the average energy of the electrons, as given by the hot-electron temperature. For the experiments presented in this work, we estimate (self-consistently, from the results of this calculation) that N_e is about 10^{14} to 10^{15}. Next, we obtained the volume by taking the product of the surface area of the cone and the characteristic scale length along the expansion dimension, given by $\approx c \times \tau_L$. The hot-electron density is then just the ratio of the number of hot electrons to volume. Since the plasma frequency ultimately depends on the hot-electron temperature through the density, Eq. (1) is transcendental and must be solved numerically.

It is important to recognize that the density computed here ($n_{e0} \sim 10^{17}$ cm^{-3}) is an overestimate. As discussed in **Source of the Protons** (p. 208), these protons are accelerated from the surfaces of the cone, possibly by hot-electron return currents. In the calculation, we assumed that the hot-electron density is uniform, which is generally not the case. We expect the hot-electron densities to be lower upstream of the cone tip, where the ions are accelerated. In addition, if the protons are indeed accelerated by hot-electron return currents, we expect these currents to be colder and less dense than the initial forward current. From Eq. (1), it is evident that for a given maximum proton energy, an upper bound on n_{e0}, and therefore on ω_{pi}, corresponds to a *minimum* inferred hot-electron temperature.

Even though these ion expansion models apply primarily to thin-foil experiments,[11,12] they can be used in the context of this work. A major distinction, however, between thin-foil experiments and those presented here must be considered to allow for a correct interpretation of the data taken in this work. The scale length of the ion front where the protons are accelerated is very different in these experiments. The two-phase model used here assumes that the initial scale length of this front is small in comparison to the hot-electron Debye length. While this is true for typical thin-foil experiments with short-pulse lasers, in our case the scale length of the blowoff plasma in front of the cone is ~400 μm to 1 mm due to the long-pulse laser's interaction with the capsule. The effective scale length seen by the accelerating protons is roughly of this order, whereas the hot-electron Debye length is ~20 μm. In this case, the maximum proton energy scales inversely with the initial density scale length at the ion front;[27] therefore, the proton energies shown in Fig. 132.24 are significantly lower than that expected by the model. To quantify this difference to some extent, it has been shown that the addition of a 100-μm-scale-length plasma at the ion expansion front (in a scale length otherwise dominated by the much smaller hot-electron Debye length), reduced the observed maximum proton energies by about 4× (Ref. 27). Therefore, in applying the expansion model to these experiments, it is expected that the actual temperatures are much higher than the temperature inferred using the model.

We used protons at 80° to infer the hot-electron temperature. For each shot, Eq. (1) was solved numerically for the minimum inferred hot-electron temperature, shown in Fig. 132.28. The error bars correspond to the uncertainty of the maximum proton energy measurement. The ponderomotive vacuum scaling (for the case of negligible pre-plasma) is shown alongside these data. The minimum inferred temperatures are factors of 2 to 3 higher than the vacuum scaling. If this inferred increase in temperature is due entirely to laser self-focusing in the pre-plasma, this result corresponds to a 3 to 10× enhancement of the incident laser intensity.

It is worth noting that OMEGA EP is known to produce maximum proton energies that are higher in comparison to those of other laser systems.[28] In particular, it has been shown that for a fixed laser intensity (~2 to 8×10^{18} W/cm^2), the maximum proton energy increases as the pulse duration is increased from 1 ps to 10 ps (Ref. 29). Observations indicate that the maximum proton energy increases faster with the laser-pulse duration than models [for example, Eq. (1)] predict. At present, there is no explanation for this observation. We speculate that the effect itself could be caused by hotter electron temperatures (for instance, enhanced absorption or hot-electron refluxing) for longer pulses (10 ps) or by additional physics of the ion acceleration process that is not incorporated into the models at this point. In the context of this work, the effect of the former would be to reinforce our argument about enhanced temperatures. The effect of the latter, if present, would be to compete with the effect of the initial scale length on maximum energies; if taken into account, it would act to lower the minimum temperatures inferred in this work.

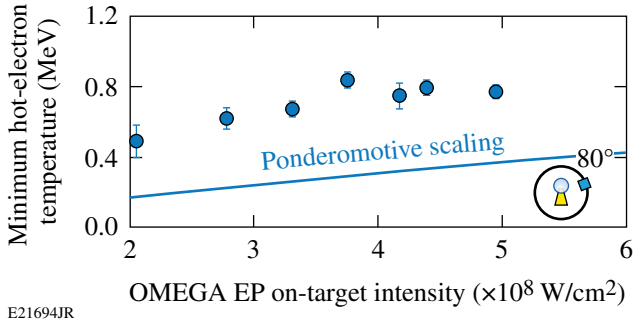

Figure 132.28
Proton-inferred hot-electron temperatures as a function of the incident short-pulse laser intensity. These temperatures are an underestimate and therefore represent the minimum initial hot-electron temperature. Shown alongside the data is the ponderomotive prediction of the hot-electron temperature for the case of negligible preformed plasma inside the cone. These inferred temperatures are 2× to 3× higher than expected.

Conclusion

This work has for the first time characterized the energy loss to fast protons in cone-in-shell fast-ignitor experiments. We estimate that of the order of 10 J, or 1% of the short-pulse laser energy, is lost to fast protons. It has been shown that these protons are accelerated from the entire surface of the cone, rather than from the cone tip alone. Since these protons are accelerated far upstream from where the short-pulse laser interacts with the tip, one possibility is that they are accelerated by hot-electron return currents. This notion is further corroborated by the fact that proton acceleration depends on the integrity of the cone tip.

Finally, these protons have been used to estimate a lower bound on the initial hot-electron temperature. These minimum, proton-inferred hot-electron temperatures (500 to 900 keV) are hotter than predicted from the ponderomotive scaling by factors of 2 to 3. If the enhancement of the hot-electron temperature is due entirely to laser self-focusing, this result corresponds to a minimum enhancement of 3× to 10× the incident laser intensity.

ACKNOWLEDGMENT

This work was supported in part by the Fusion Science Center (Rochester Sub Award PO No. 415023-G), National Laser Users' Facility (DOE Award No. DE-NA0000877), U.S. DOE (Grant No. DE-FG52-09NA29553), Laboratory for Laser Energetics (LLE) (No. 414090-G), and Lawrence Livermore National Laboratory (No. B580243).

REFERENCES

1. N. G. Basov, S. Yu. Gus'kov, and L. P. Feokistov, J. Sov. Laser Res. **13**, 396 (1992).
2. M. Tabak *et al.*, Phys. Plasmas **1**, 1626 (1994).
3. D. G. Hicks, C. K. Li, F. H. Séguin, J. D. Schnittman, A. K. Ram, J. A. Frenje, R. D. Petrasso, J. M. Soures, D. D. Meyerhofer, S. Roberts, C. Sorce, C. Stoeckl, T. C. Sangster, and T. W. Phillips, Phys. Plasmas **8**, 606 (2001).
4. A. B. Zylstra *et al.*, Phys. Plasmas **19**, 042707 (2012).
5. P. McKenna *et al.*, Phil. Trans. R. Soc. A **364**, 711 (2006).
6. S. S. Bulanov *et al.*, Phys. Rev. E **78**, 026412 (2008).
7. K. A. Flippo *et al.*, Phys. Plasmas **15**, 056709 (2008).
8. P. Mora, Phys. Rev. Lett. **90**, 185002 (2003).
9. P. Mora, Phys. Rev. E **72**, 056401 (2005).
10. P. Mora, Phys. Plasmas **12**, 112102 (2005).
11. J. Fuchs *et al.*, Nat. Phys. **2**, 48 (2006).

12. L. Robson *et al.*, Nat. Phys. **3**, 58 (2007).

13. T. R. Boehly, D. L. Brown, R. S. Craxton, R. L. Keck, J. P. Knauer, J. H. Kelly, T. J. Kessler, S. A. Kumpan, S. J. Loucks, S. A. Letzring, F. J. Marshall, R. L. McCrory, S. F. B. Morse, W. Seka, J. M. Soures, and C. P. Verdon, Opt. Commun. **133**, 495 (1997).

14. L. J. Waxer, D. N. Maywar, J. H. Kelly, T. J. Kessler, B. E. Kruschwitz, S. J. Loucks, R. L. McCrory, D. D. Meyerhofer, S. F. B. Morse, C. Stoeckl, and J. D. Zuegel, Opt. Photonics News **16**, 30 (2005).

15. W. Theobald, A. A. Solodov, C. Stoeckl, K. S. Anderson, R. Betti, T. R. Boehly, R. S. Craxton, J. A. Delettrez, C. Dorrer, J. A. Frenje, V. Yu. Glebov, H. Habara, K. A. Tanaka, J. P. Knauer, R. Lauck, F. J. Marshall, K. L. Marshall, D. D. Meyerhofer, P. M. Nilson, P. K. Patel, H. Chen, T. C. Sangster, W. Seka, N. Sinenian, T. Ma, F. N. Beg, E. Giraldez, and R. B. Stephens, Phys. Plasmas **18**, 056305 (2011).

16. F. H. Séguin, J. A. Frenje, C. K. Li, D. G. Hicks, S. Kurebayashi, J. R. Rygg, B.-E. Schwartz, R. D. Petrasso, S. Roberts, J. M. Soures, D. D. Meyerhofer, T. C. Sangster, J. P. Knauer, C. Sorce, V. Yu. Glebov, C. Stoeckl, T. W. Phillips, R. J. Leeper, K. Fletcher, and S. Padalino, Rev. Sci. Instrum. **74**, 975 (2003).

17. N. Sinenian *et al.*, Rev. Sci. Instrum. **82**, 103303 (2011).

18. D. G. Hicks, C. K. Li, F. H. Séguin, A. K. Ram, J. A. Frenje, R. D. Petrasso, J. M. Soures, V. Yu. Glebov, D. D. Meyerhofer, S. Roberts, C. Sorce, C. Stöckl, T. C. Sangster, and T. W. Phillips, Phys. Plasmas **7**, 5106 (2000).

19. P. M. Nilson, A. A. Solodov, J. F. Myatt, W. Theobald, P. A. Jaanimagi, L. Gao, C. Stoeckl, R. S. Craxton, J. A. Delettrez, B. Yaakobi, J. D. Zuegel, B. E. Kruschwitz, C. Dorrer, J. H. Kelly, K. U. Akli, P. K. Patel, A. J. Mackinnon, R. Betti, T. C. Sangster, and D. D. Meyerhofer, Phys. Rev. Lett. **105**, 235001 (2010).

20. S. P. Hatchett, C. G. Brown, T. E. Cowan, E. A. Henry, J. S. Johnson, M. H. Key, J. A. Koch, A. B. Langdon, B. F. Lasinski, R. W. Lee, A. J. MacKinnon, D. M. Pennington, M. D. Perry, T. W. Phillips, M. Roth, T. C. Sangster, M. S. Singh, R. A. Snavely, M. A. Stoyer, S. C. Wilks, and K. Yasuike, Phys. Plasmas **7**, 2076 (2000).

21. S. C. Wilks *et al.*, Phys. Plasmas **8**, 542 (2001).

22. J. Li, J. Davies, C. Ren, A. Solodov, W. Theobald, J. Tonge, and W. Mori, Bull. Am. Phys. Soc. **56**, 222 (2011).

23. C. Stoeckl, M. Cruz, V. Yu. Glebov, J. P. Knauer, R. Lauck, K. Marshall, C. Mileham, T. C. Sangster, and W. Theobald, Rev. Sci. Instrum. **81**, 10D302 (2010).

24. A. A. Solodov, K. S. Anderson, R. Betti, V. Gotcheva, J. F. Myatt, J. A. Delettrez, S. Skupsky, W. Theobald, and C. Stoeckl, Phys. Plasmas **16**, 056309 (2009).

25. C. D. Zhou, W. Theobald, R. Betti, P. B. Radha, V. A. Smalyuk, D. Shvarts, V. Yu. Glebov, C. Stoeckl, K. S. Anderson, D. D. Meyerhofer, T. C. Sangster, C. K. Li, R. D. Petrasso, J. A. Frenje, and F. H. Séguin, Phys. Rev. Lett. **98**, 025004 (2007).

26. P. Mora, in *Asian Summer School on Laser Plasma Acceleration and Radiation*, edited by Z.-M. Sheng and J. Zhang (AIP, New York, 2007), Vol. 920, pp. 98–117.

27. A. J. Mackinnon *et al.*, Phys. Rev. Lett. **86**, 1769 (2001).

28. K. Flippo, T. Bartal, F. Beg, S. Chawla, J. Cobble, S. Gaillard, D. Hey, A. MacKinnon, A. MacPhee, P. Nilson, D. Offermann, S. Le Pape, and M. J. Schmitt, J. Phys., Conf. Ser. **244**, 022033 (2010).

29. L. Gao, P. M. Nilson, W. Theobald, C. Stoeckl, C. Dorrer, T. C. Sangster, D. D. Meyerhofer, L. Willingale, and K. M. Krushelnick, Bull. Am. Phys. Soc. **55**, 377 (2010).